Disentangling Memristive and Memcapacitive Effects in Droplet Interface Bilayers using Dynamic Impedance Spectroscopy

Robert L. Sacci,[1] Haden L. Scott,[2] Zening Liu,[3] Dima Bolmatov,[4] Benjamin Doughty,[1] John Katsaras,[4,5]* C. Patrick Collier[3]**

[1]Chemical Sciences Division, Oak Ridge National Laboratory, Oak Ridge, Tennessee 37831
[2]Large Scale Structures, Neutron Scattering Division,
Oak Ridge National Laboratory, Oak Ridge, Tennessee 37831
[3]Center for Nanophase Materials Sciences,
Oak Ridge National Laboratory, Oak Ridge, Tennessee 37831
[4]Labs and Soft Matter Group, Neutron Scattering Division,
Oak Ridge National Laboratory, Oak Ridge, Tennessee 37831
[5]Shull Wollan Center, Oak Ridge National Laboratory, Oak Ridge, Tennessee 37831

Keywords: lipid bilayer, dynamic impedance spectroscopy, nonlinear elements, memristor, memcapacitor, droplet interface bilayer

This manuscript has been authored by UT-Battelle, LLC, under contract DE-AC05-00OR22725 with the US Department of Energy (DOE). The US Government retains and the publisher, by accepting the article for publication, acknowledges that the US government retains a nonexclusive, paid-up, irrevocable, worldwide license to publish or reproduce the published form of this manuscript or allow others to do so, for US government purposes. DOE will provide public access to these results of federally sponsored research in accordance with the DOE Public Access Plan (http://energy.gov/downloads/doe-public-access-plan).

Disentangling Memristive and Memcapacitive Effects in Droplet Interface Bilayers using Dynamic Impedance Spectroscopy

Robert L. Sacci,[1*] *Haden L. Scott,*[2] *Zening Liu,*[3] *Dima Bolmatov,*[4] *Benjamin Doughty,*[1] *John Katsaras,*[4,5*] *C. Patrick Collier*[3*]

[1]Chemical Sciences Division, Oak Ridge National Laboratory, Oak Ridge, Tennessee 37831
[2]Large Scale Structures, Neutron Scattering Division,
Oak Ridge National Laboratory, Oak Ridge, Tennessee 37831
[3]Center for Nanophase Materials Sciences,
Oak Ridge National Laboratory, Oak Ridge, Tennessee 37831
[4]Labs and Soft Matter Group, Neutron Scattering Division,
Oak Ridge National Laboratory, Oak Ridge, Tennessee 37831
[5]Shull Wollan Center, Oak Ridge National Laboratory, Oak Ridge, Tennessee 37831

*saccirl@ornl.gov
*katsarasj@ornl.gov
*colliercp@ornl.gov

Keywords: lipid bilayer, dynamic impedance spectroscopy, nonlinear elements, memristor, memcapacitor, droplet interface bilayer

Abstract

The underlying principles for generating intelligent behavior in living organisms are fundamentally different from those in traditional solid-state circuits. Biomimetic neuromorphic equivalents based on biological membranes offer novel implementation of tunable plasticity and diverse mechanisms to control functionality. Here, we used dynamic electrochemical impedance spectroscopy (dEIS) to probe diphytanoylphosphatidylcholine (DPhPC) droplet interface bilayers (DIBs) to better understand the differences in molecular level structure/dynamics that give rise to hysteretic loops and neuromorphic, memelement behaviors in lipid bilayers in response to electrical biasing. Importantly, this system does not have ion-conducting channels and was therefore, not expected to show memristive behavior. Surprisingly, we detected both memristive and memcapacitive behaviors by measuring the time-dependent complex impedance of DPhPC DIBs. We show that nonlinear memristance can originate from structural changes in the bilayer, affecting its dielectric properties. This novel dEIS application allows for the simultaneous analysis of the system's changing memristive and memcapacitive properties, which originate from different molecular restructuring processes. Moreover, and importantly, access to this type of information increases the number of neuromorphic processes supported simultaneously in a single two-terminal device.

Introduction

Lipids are amphipathic biomolecules that make up a significant proportion of biological membranes. In their purified forms, they self-assemble into various morphologies (cubic, hexagonal, lamellar, *etc*.),[1] with the lamellar phase considered the most biologically relevant.[2] In many ways, membranes are the gate-keepers to cell interiors and are responsible for cell-cell recognition, protein sorting, cellular protection, and signaling, to name a few.[3] Lipids also account for about 50% of the brain's dry weight and they vary spatially from one region of the brain to another.[4] Moreover, the lipid composition of neuronal cell membranes affects their function and, ultimately, the brain's ability to reconfigure neuronal connectivity.[5] Of significance, however, is the fact that the brain's synaptic plasticity, or its ability to adapt and perform complex parallel operations with minimum power requirements,[6,7] is unlike anything currently used in state-of-the-art complementary metal-oxide-semiconductors (CMOS) technologies trying to mimic its dynamics and tunable functionality. Understanding how the brain manages its more than 600 trillion synapses, each requiring dynamic molecular reconfiguration while consuming very little power, will undoubtedly lead to the production of low-power, neuromorphic computing systems based on soft materials, not unlike those found in the brain.

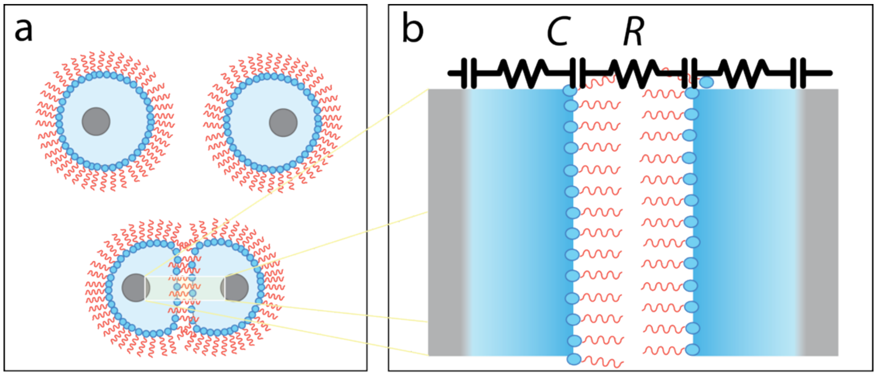

Figure 1. Illustration of (a) droplet interface bilayer (DIB) and, (b) a close-up view of the lipid bilayer, along with a common equivalent circuit model used for characterizing it.

When two lipid-coated aqueous droplets in an oil phase are brought together they can form a droplet interface bilayer or DIB, **Figure 1**.[8] These bilayers can be chemically symmetric or asymmetric and include integral pore-forming peptides and proteins, such as alamethicin ion channels.[9] DIBs, therefore, offer a membrane platform that is readily tunable and can mimic membranes found in living systems. Recently, we reported on DIBs doped with alamethicin ion channels that demonstrated memristive behavior, characterized by pinched hysteresis in the current-voltage plane, and memcapacitive behavior, characterized by pinched hysteresis in the charge-voltage plane. These membranes had the ability to emulate key synaptic functions, such as pulsed-pair facilitation and depression in memristors, and activity-dependent dynamical changes in the capacitance of memcapacitors,[9,10] signatures of neuromorphic processing in the form of short-term synaptic plasticity.

These soft matter-based memory devices operate using small voltage signals (50-100 mV), which are smaller than those required by two-terminal solid-state memristive devices such as conductive filament or phase change memory memristive devices (0.5 to 5 V), [11,12] DIBs are two terminal neuromorphic devices that show memelement properties directly through the nanoscale reorganization of the bilayer in response to changes in the interfacial charge density, without the need for a third gate terminal to control switching and memory storage in low-power organic neuromorphic devices based on transistor geometries.[13] These molecular-scale perturbations also result in time-dependent changes in electrical capacitance. In other words, there are two interconnected processes taking place on different timescales, which enable biomimetic memory in response to electrical signals: *e.g.*, mesoscale geometrical changes in membrane area and thickness of the lipid bilayer between the two droplets in a DIB due to electrowetting[9] and electrocompression,[10] and double layer charging, ionic transport, and molecular-scale rearrangements in the membrane, which include (de)solvation, densification, and head group reorientation.

In this work, we used diphytanoylphosphatidylcholine (DPhPC) DIBs immersed in hexadecane and dynamic electrochemical impedance spectroscopy (dEIS) to explicitly probe the bilayer's response to individual sinusoidal frequencies and time-dependent impedance. Electrochemical impedance spectroscopy (EIS) measures the frequency response of an electrochemical system, including its energy storage and dissipation properties.[14] However, since EIS measures the electrical properties of the system under steady state conditions, it is therefore unable to provide information about the dynamics of the system in the time domain. On the other hand, dEIS interrogates the *temporal* development of kinetics and dynamics in electrochemical systems, such as DIBs, by applying a multi-sine probe to monitor changes in the frequency-resolved electrical responses (impedance) as functions of time.[15-18] Analysis of the dynamic complex impedance spectra enables observation of time-dependent capacitance and resistance changes that give rise to the pinched hysteresis observed in these memelements.

The DPhPC DIB system used here does not contain ion channels and is known to show high resistance (>1 MΩ); however, memristance behavior is still possible if the dielectric loss of the bilayer changes due to head group reorganization or tail rearrangement. For example, consider the case of a typical dynamical response measurement of a bilayer without ion channels, where a single bipolar AC voltage $[E(t) = E_{\mathrm{amp}}\sin(2\pi f t)]$ is applied along with a small amplitude, high-frequency triangular voltage probe signal to monitor the differential capacitance, given by:[10]

$$C_{diff}(E) = \frac{|I(E) - I_{\mathrm{average}}(E)|}{s}, \tag{1}$$

where s is the triangle probe signal's sweep rate (V/s) and $|I(E) - I_{\mathrm{average}}(E)|$ is the resulting square wave current to the triangular probe voltage. This method is conducive to measuring "pinched hysteresis" I-E curves that are indicative of memristive systems and similar curves of electric charge (q) vs voltage for memcapacitive systems.[19,20] However, for less ideal or more complicated systems that show a variety of behaviors, distinguishing memristance from memcapacitance becomes more complicated because the current decay profile is convoluted in the time domain.[18] Explicitly probing the response of multiple sinusoidal frequencies allows for analysis in frequency-space, enabling deconvolution of electrical elements like capacitors and resistors.[16-18, 21] Here, we utilize dEIS to disentangle the system's memristive and memcapacitive properties arising from molecular and conformational changes in the lipid bilayer. By separating these processes, we provide: (1) new insights into the design of new neuromorphic devices; (2) an understanding as to how to build multiple memelement functionalities into a single two-terminal device; (3) demonstration of memristive behavior from dielectric loss change and not solely ion transport through the bilayer; and (4) a proof-of-principle demonstration for the use of dEIS in evaluating the next-generation of biomimetic electronic devices.

Experimental Methods

Materials. 1,2-diphytanoyl-sn-glycero-3-phosphocholine (DPhPC) was purchased from Avanti Polar Lipids (Alabaster, AL) and used as supplied. H_2O was obtained from a High-Q purification system (Wilmette, IL). 3-(N-morpholino) propanesulfonic acid (MOPS, $\geq$99.5%) and potassium chloride (KCl, 99.0-100.5%) (Sigma-Aldrich, St. Louis, MO) were used to prepare the aqueous buffering solution. Sodium hydroxide was purchased from Sigma-Aldrich (St. Louis, MO) and was used to adjust the pH of the buffering solution to pH 7.4. Silver/silver chloride (Ag/AgCl) electrodes were constructed by heating 125 μm diameter Ag wires (Goodfellow) to form ball terminations and then soaked in bleach. The ball ends of the wires were coated with 1% agarose (ThermoFisher Scientific, Waltham, MA). Clear photopolymer resin was purchased from FormLabs Inc. (Somerville, MA) to 3D print transparent reservoirs that were filled with hexadcane ($\geq$99%, Sigma-Aldrich).

Vesicle preparation and DIB assembly. DPhPC multilamellar vesicles (MLVs) were prepared by hydrating a dried film of DPhPC with 10mM MOPS and 500mM KCl buffer prepared in H_2O at pH 7.4. The MLV solution was then sonicated for 30 minutes, followed by six freeze/thaw cycles (-80°C, 40°C). To generate the large unilamellar vesicles (LUVs, liposomes) needed for DIBs, sonicated lipid was extruded through a polycarbonate membrane with 100 nm diameter pores (31 passes) using an Avanti Mini Extruder (Avanti Polar Lipids, Inc., Alabaster, AL). The final lipid concentration was 2 mg/mL. DIBs were formed by suspending the electrodes over a 3D-printed stadium (Formlabs Form 2, Somerville, MA) filled with hexadecane using micro-manipulators. The agarose-coated ball ends of the Ag/AgCl electrodes were submerged into the hexadecane and then 300 nL aqueous droplets containing the liposomes were pipetted onto the ball ends of each electrode. A lipid monolayer at the interface between the oil and aqueous solutions was allowed to form during an incubation period. After proper lipid monolayer formation (indicated by droplets sagging on the electrodes), the droplets were brought into close contact to spontaneously form a bilayer.[10] An Evolve 512 camera (Photometrics, Tucson, AZ) mounted on a Nikon Eclipse TE300 inverted microscope (Melville, NY) was used to monitor this process in real-time. Bilayer formation was also monitored via electrical measurements, as bilayer formation leads to an increase in membrane capacitance. A 10 Hz, 10 mV triangle wave was supplied to the electrodes using a Stanford Research Systems DS345 function generator (Sunnyvale, CA) and an Axon Instruments Axopatch 200B patch clamp amplifier (Molecular Devices, San Jose, CA), giving rise to square wave response signal due to the capacitive membrane. Capacitive currents were observed in real-time using the Clampex software (Molecular Devices, San Jose, CA).

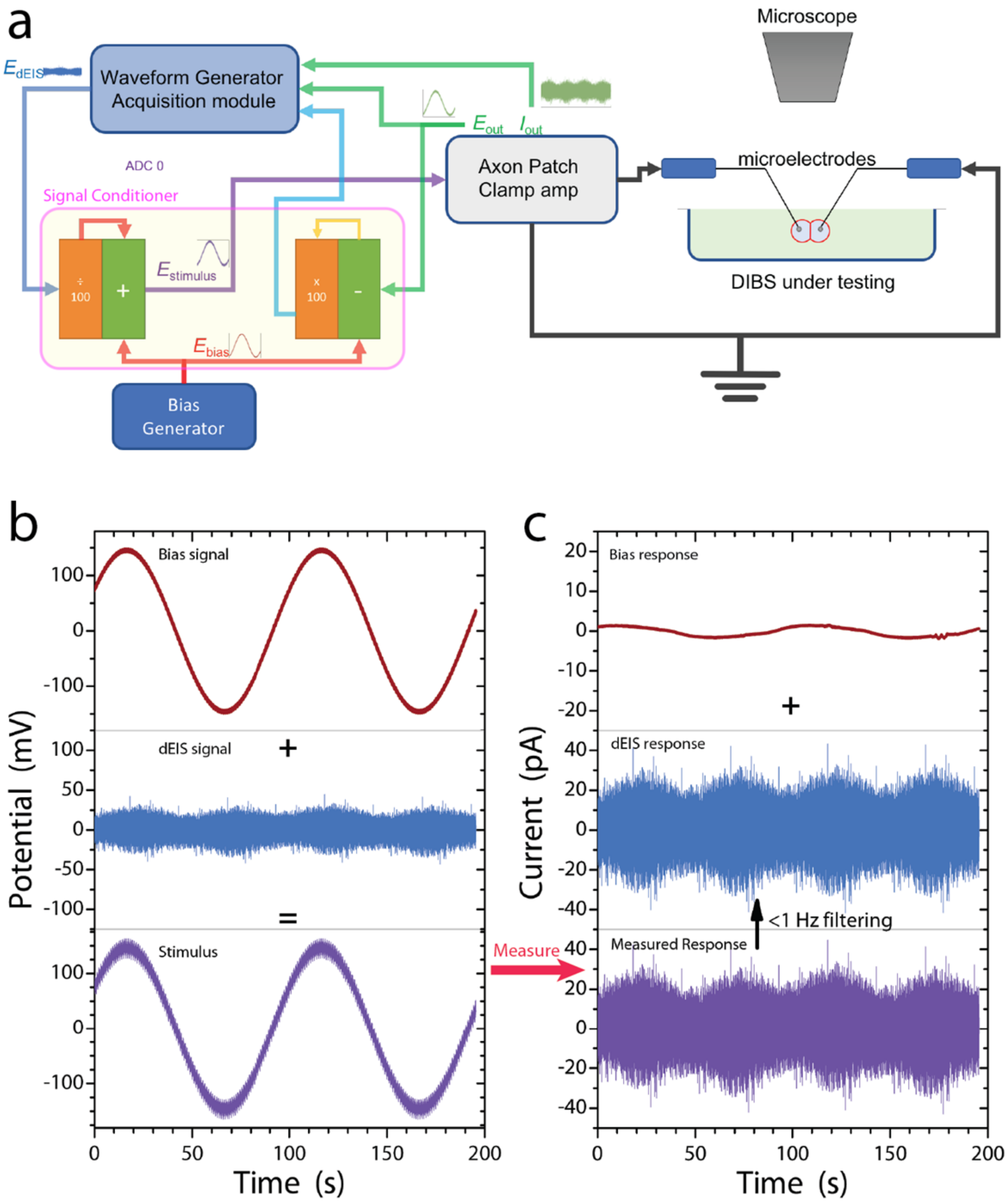

Figure 2. (a) The dEIS experimental setup used to study the DPhPC DIB system. (b) Shows the multi-sine waveform synthesis and applied stimulus, and (c) the measured response from the DPhPC DIBs system.

dEIS measurement. DIBs and measurement probes were placed inside a Faraday cage, and the entire experimental setup was attached to an anti-vibration isolation table to minimize external noise and vibrations. **Figure 2a** shows a schematic of our dEIS system used to study DPhPC DIBs, which is described in more detail elsewhere.[17,18] Briefly, we replaced the typical triangular waveform, described above for determining the differential capacitance, with a multi-sine waveform (shown in **Figure 2a, b)** synthesized by a KUSB-3116 waveform generator (Keithley, Beaverton, OR). This waveform was conditioned by a SRS900 mainframe (Stanford Research Systems, Sunnyvale, CA), and then added to the bias signal before being transferred to the patch clamp amplifier to apply the electrical signal to the DIB. The waveform consisted of roughly 45 frequencies between 1 and 13500 Hz or 10 and 32700 Hz. Frequency selection obeyed the following rules:[18, 22-24] (1) each selected frequency had an integer number of periods in the total waveform period as defined by the minimal frequency, *i.e.*, $T = 1/f_{\text{min}}$; (2) the frequencies followed Popkirov's prime numbers sequence to reduce harmonic and inter-harmonic overlap; (3) the amplitudes for individual sine waves decreased by half for every decade increase in frequency; (4) phases were random; and (5) the maximum amplitude of the waveform was ~ 20 mV. The signal conditioner was used to add the waveform to the biasing signal (Figure 2a, b) and then apply it to the DIB. The potential and current were continuously sampled from the patch clamp and digitized by the KUSB-3116 acquisition module at a rate of 98 kHz (Fig. 2a,c). After measurement, the raw data was transformed into the frequency domain using a sliding window Fast Fourier Transform (FFT) algorithm, which also deconvoluted the "DC" or zeroth frequency response from the dEIS signal (Figure 2c). Representative potential and current FFT results are shown in **Figure 3**. We numerically converted the real and imaginary FFT results into complex impedance, *Z*, using the expression,

$$Z = \frac{(E_{\mathrm{r}}I_{\mathrm{r}} + E_{\mathrm{i}}I_{\mathrm{i}}) + \mathrm{i}(E_{\mathrm{i}}I_{\mathrm{r}} - E_{\mathrm{r}}I_{\mathrm{i}})}{(I_{\mathrm{r}}^2 + I_{\mathrm{i}}^2)}, \qquad (2)$$

where the subscripts *r* and *i* denote the real and imaginary parts of the potential (*E*) and current (*I*) signals. We extracted only the frequencies that corresponded to those used to synthesize the multi-sine waveform. Notably, we found no evidence of nonlinear response from the probe waveform using harmonic detection, indicating that the time-resolved impedance spectra could be analyzed using a linear equivalent circuits analysis. We used ZView (Scribner Associates, Southern Pines, NC) software to batch-fit the impedance spectra to a simple *RC*-circuit model. Examples of fitting two time-resolved impedance spectra are shown in Figure 3b.

Theory

As mentioned, we have previously used DIBs (Figure 1a) as platforms for neuromorphic memelement circuits.[8-10] Electroanalytical techniques were used to determine and disentangle information about charge storage at interfaces with ion transport through layers and across boundaries. For example, in a bilayer system, there are two interfaces (lipid/water) and two phases (lipid and water), which correspond to capacitors and resistors in an equivalent circuit analysis (Figure 1b).[11,22] Assuming no charge transfer reactions or the occurrence of complete desolvation, resistors and capacitors add together to give a single *RC* circuit. For linear circuits, these elements are independent of applied voltage and history. Such a system is thus expected to show a single time-independent time constant, $\tau = RC$.

An essential aspect of a dEIS measurement is that the system response is slower than the slowest frequency component in the waveform, f_{min}. Classical EIS provides frequency-resolved information on the system's complex impedance response under steady-state conditions.[24] While EIS can be used to probe changes in C_{diff} or R_{diff}, the fact that it's a steady-state measurement limits its use for neuromorphic systems as compared to those with sufficiently long memory times (*e.g.*, minutes to hours).[25] However, dEIS utilizes a complex waveform that modulates the system at higher frequencies than the carrier (driving) signal to construct the time-resolved impedance, which follows changes in DIB impedance as a function of potential sweep rate and holding time.[17,18,26-28] Underkofler and Shain proposed the boundary condition that the sweep rate should be “much slower” than f_{min}.[29] Garland et al. experimentally determined that the change in the current response is also important:[24]

$$f_{\text{min}} \gg \left(\frac{dI}{dt}\right)\Delta I_{\text{rms}} \tag{3}$$

Later, Sacci and Harrington added a pair of conditions that further expounded on the mechanistic nature of Garland’s condition, namely, that the change in surface coverage, θ, (related to R_{diff} in an interfacial reaction) and slowest reaction/process time constants measurable (which are related to changes in C_{diff} and R_{diff}) must also be much slower than f_{min}.[18]

$$f_{\text{min}} \gg \left(\frac{d\theta}{dt}\right)\Delta\theta_{\text{rms}} \tag{4}$$

$$f_{\text{min}} \gg \tau^{-1} \tag{5}$$

Experimentally, “much slower” means at least one order of magnitude slower. If these conditions are met, the dEIS measurement approximates a steady-state condition, where the system is linear, causal, stable, and finite within the waveform period, and the complex data will obey the Kramers-Kronig relationship.[30, 31] Note, however, that these kinetic and mechanistic parameters are not known *a priori*. Therefore, baseline measurements should be performed to estimate the dEIS frequency bandwidth that will provide meaningful data.

In the above-described example, the complex impedance is directly related to the differential (or dynamical) resistance and capacitance, as:

$$Z(t) = \frac{\partial I}{\partial E} = R_{\text{diff}}(t) - \mathrm{i}(2\pi f\, C_{\text{diff}}(t))^{-1}. \tag{6}$$

This suggests that hysteresis in an *I-E* or *q-E* curve during a time-dependent bias protocol should correspond to hysteresis in the impedance. In other words, any voltage or surface charge-induced change can result in a change in R_{diff}, C_{diff}, or both.

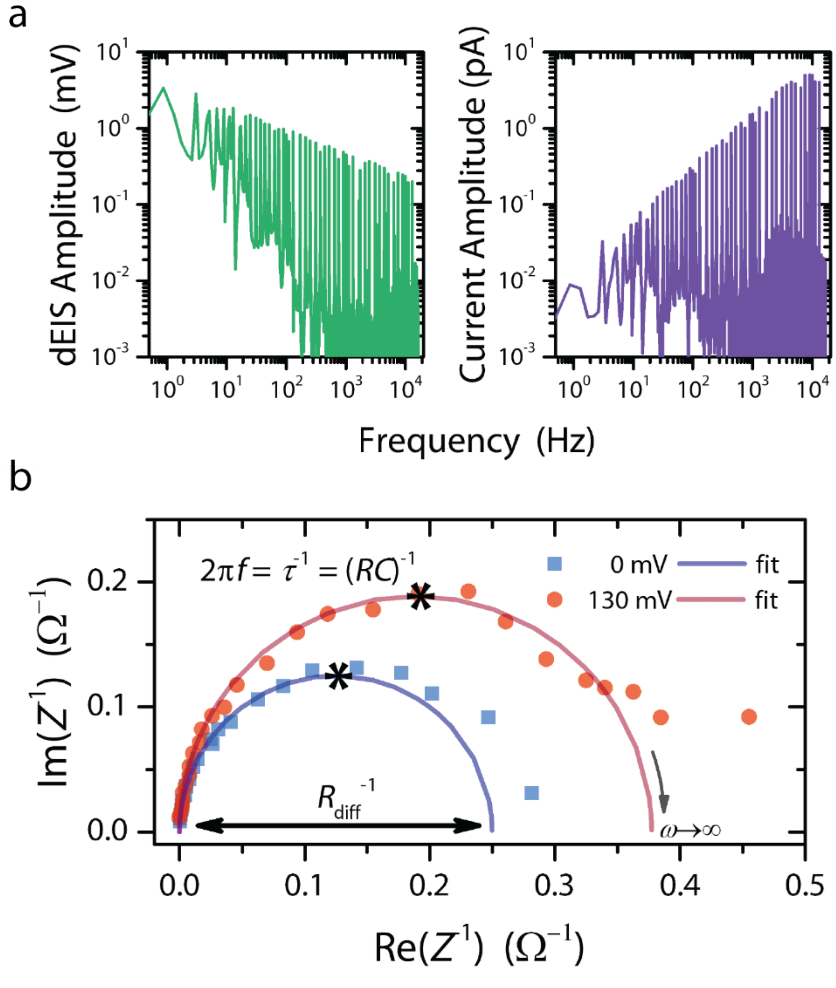

Figure 3. (a) Representative potential and current FFT spectra from the raw signals shown in Figure 1. (b) Representative dEIS spectra measured at 0 and 130 mV during a 10 mHz biasing scan, and corresponding *RC*-circuit fitting results. The complex impedance is presented in the reciprocal plane to highlight changes to the system.

Equation 6 suggests that the complex impedance provides a means to deconvolute the differential capacitance and resistance; C_{diff} is related to how the imaginary impedance changes with frequency, and R_{diff} is related to the shift in the real impedance. Figure 3b provides an example of the complex impedance measured using dEIS. For clarity, we plot the impedance in reciprocal space (typically referred to as admittance). Fitting the data to an equivalent circuit model with the frequency-resolved complex impedance increases measurement certainty and reveals the "quality" of the bilayer, *e.g.*, if it is leaky. The high frequency region (>10 kHz) appears noisy and may be due to bandwidth limitations of the Axopatch 200B patch clamp amplifier. A change in R_{diff} (related to the reciprocal diameter of the semicircle) can be indicative of a change in dielectric loss or charge transport through the DIB. In contrast, a change in C_{diff} (related to the frequency at the semicircles' maxima, indicated by asterisks) is associated with a structural change in the bilayer interface or thickness.[30-32] Given that DPhPC DIBs do not contain protein or peptide ion channels, R_{diff} is better described by dielectric loss rather than charge transport resistance. Figure 3b clearly shows that biasing the bilayer from 0 to 130 mV caused a change in the semicircle diameter and a shift in the peak frequency. This frequency shift is indicative of not only a change in capacitance, but also in the electrical time constant, τ, of the RC circuit that describes the membrane (such as that depicted in Figure 1), as given by:

$$\tau = RC_{\text{tot}} = \frac{\rho\, l \varepsilon_{\text{r}} \varepsilon_0\, A}{A \quad l} = \rho \varepsilon_{\text{r}} \varepsilon_0 \quad , \tag{7}$$

where l and A are the bilayer thickness and area, respectively, ρ is the specific resistivity $\left(\rho = \frac{RA}{l}\right)$, and ε_{r} is the effective permittivity $\left(\varepsilon_{\text{r}}\varepsilon_0 = \frac{C_{\text{tot}} l}{A}\right)$. The total capacitance, C_{tot}, is the sum of all the charge storage processes at the membrane, including ionic adsorption-trapping at the headgroups, inner and diffuse electrochemical double layers, and membrane dielectric response, described by:

$$\frac{1}{C_{\text{tot}}} = \frac{1}{C_{\text{ads}}} + \frac{1}{C_{\text{dl}}} + \frac{1}{C_{\text{dipole}}} \, . \tag{8}$$

The effective permittivity of the DIBs thus includes contributions from these above-described terms, causing shifts in τ. In Equation 7, R and C_{tot} are inverse functions of the bilayer geometry. That is, if A increases, C_{tot} increases but R decreases. Changes in bias potential drive these geometric changes via voltage-dependent electrostriction effects that act on lipid bilayers, including electrowetting[9] and electrocompression.[10] These *mesoscale* processes are driven by interfacial tension and inter-drop adhesion energies.

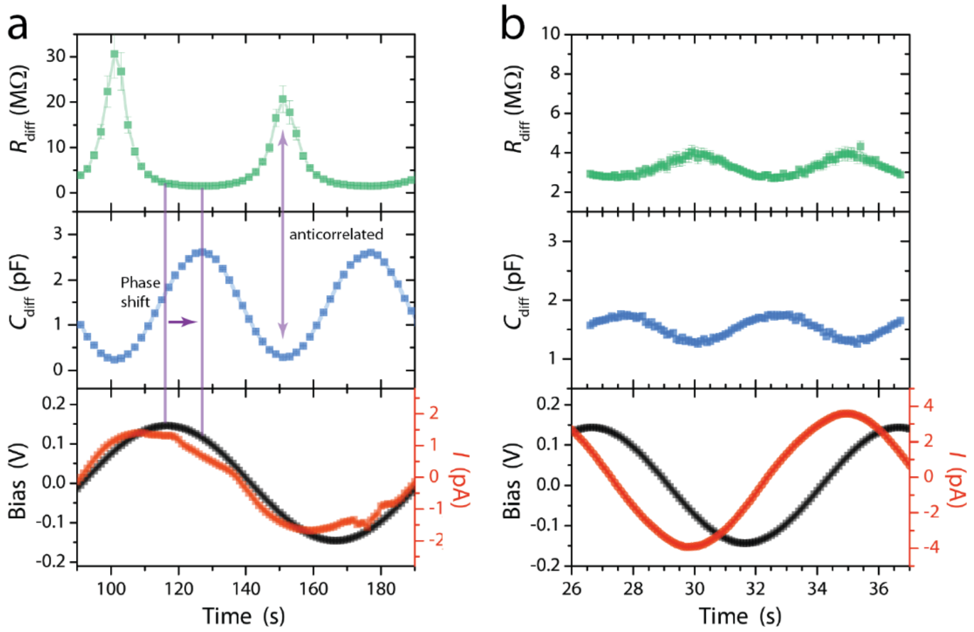

Figure 4. Time-resolved differential resistance and capacitance obtained by fitting dEIS spectra along with the carrier signal and the average current response. (a) 10 mHz and (b) 100 mHz carrier signals.

On the other hand, τ is independent of changes to the bilayer geometry terms, which cancel in Equation 7, leaving $\tau = \rho\varepsilon_r\varepsilon_0$, with units of time (seconds). This indicates that time constants are changing because of electrically induced structural changes taking place at the *molecular* level, such as (de)solvation, changes in water-lipid interactions, or transient pore formation, all of which affect the bilayer's dielectric properties (*i.e.*, $\varepsilon_r\varepsilon_0$ changes). In other words, detecting dynamic changes in both capacitance and resistance at the same time, allows for the simultaneous detection of subtle memelement behaviors having different molecular origins.

Results and Discussion

Figure 4 shows typical memcapacitive and memristive responses originating from dEIS measurements using 10 and 100 mHz sinusoidal carrier signals and biasing between -150 and +150 mV.[9] For both frequencies, the differential resistance (R_{diff}) and capacitance (C_{diff}) are out of phase from one another and show a doubling of the carrier frequency. We also observe a phase shift of

~ 0.1 rad in both R_{diff} and C_{diff} relative to the bias for both frequencies (10 and 100 mHz). The two significant differences between the low and high frequencies are: (1) the zeroth frequency current (I) oscillations become distorted at 10 mHz compared to 100 mHz; and (2) R_{diff} at 10 mHz is no longer sinusoidal in shape, having now sharp peaks that are an order of magnitude greater than the baseline. These differences are suggestive of nonlinear behavior in the low-frequency biasing condition. We note that the zeroth frequency current in Figure 4a does not cross 0 pA at 0 mV (Figure S1a) and so does not demonstrate the zero-crossing pinched hysteresis in the I-E plane, a fingerprint of an ideal memristive system in this frequency range.[19] Likewise, there is no zero-crossing pinched hysteresis in the q-E plane describing an ideal memcapacitive system (Figure S1b). However, the lack of a clear pinched hysteresis, in both cases, is likely due to the time-domain current signal (Figure 4a) becoming saturated with perturbations from over 40 separate sinusoidal waveforms (see Figure 2). Similar behavior has been reported for several electrochemical systems, both in the time domain using I-E scans,[32-34] and in the frequency domain with EIS,[35] and have been attributed to capacitively and inductively coupled memristive models. We also note that we had previously reported zero-crossing pinched hysteresis in the I-E and the q-E planes for the same DPhPC DIBs system as studied here, as expected for voltage-controlled memristive and memcapacitive systems.[9,10]

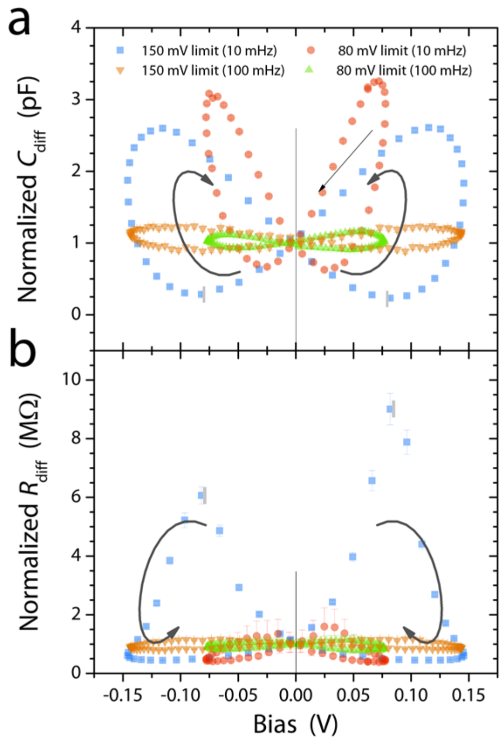

Figure 5. Frequency and bias limit dependencies of pinched hysteresis for memcapacitive and memristive DPhPC bilayers. Differential capacitance (a) and resistance (b) of a symmetric DPhPC bilayer as a function of voltage. These results show how **the system can be tuned through excitation frequency and voltage to decouple memcapacitance and memristance** to form a dual memory element system in a two-terminal device. Arrows show direction of the loop traces in time.

Figure 5 shows R_{diff} and C_{diff} hysteresis loops plotted using the data from Figure 4, in addition to results from a ± 80 mV bias voltage for comparison. Both the C_{diff} and R_{diff} curves in Figure 5a and 5b, respectively, can be described as pinched hysteresis loops with the difference between the different traces being that the C_{diff} data curve upwards, while the R_{diff} turn in a downward direction (arrows show the direction of the hysteresis loops). The C_{diff} curves in Figure 5a qualitatively match those obtained previously.[10] Figure 5a shows that both the biasing frequency and amplitude affect C_{diff}. The areas of the hysteresis loops in Figure 5a increase by 3- and 5-fold (80 mV and 150 mV amplitude signals, respectively) as the frequency decreases from 100 to 10 mHz. Figure 5b shows similar responses for the differential resistance. These results are consistent with our earlier reports describing memristance and memcapacitance in DPhPC bilayers due to reversible and hysteretic voltage-dependent geometrical changes taking place in the membrane.[9,10] The fact that C_{diff} and R_{diff} do not show the same degree of change suggests that the bias limit affects the electrical time constant, implying that this response is not merely geometric in origin.

The DPhPC bilayer does not have ion channels and therefore would not be expected to show memristance behavior due to the absence of a voltage-dependent ion-conducting pathway.[9] The memristive behaviors in Figure 4 and 5 suggest that charge transport is not the only mechanism responsible for memristance. Systems where ion transport pathways form and increase with voltage tend to show orders of magnitude increases in conductivity (decrease in resistance). Here, we see subtle changes, which are better described by changes in the dipole/charge interactions at the bilayer interfaces. That is, the increased charge density with applied bias voltage at the two interfaces of the lipid bilayer (one with excess positive charge and the other with excess negative charge) affects the total dielectric loss stemming from dipole reorientation. One would then expect that memcapacitance and memristance are coupled. However, utilizing both behaviors for enhanced memory storage would require significant differences in their voltage dependencies.

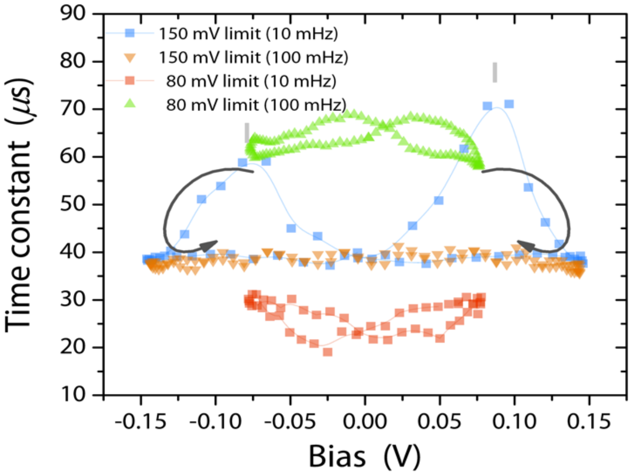

Figure 6. Electrical time constant analysis plot calculated from the product of the *C* and *R* plots in Figure 5. Average uncertainty is ~5 μs.

Figure 6 shows changes to the observed DIB charging time constant with bias voltage and frequency. Within error, τ does not change during the "high frequency" (100 mHz) 80 mV or 150 mV bias signals. However, for the "low frequency" (10 mHz) 150 mV amplitude bias, τ nearly doubles. As previously discussed, this cannot occur if the lipid bilayer experiences only charge-induced thickening/thinning (Equation 7), as observed for the 80 mV amplitude and 100 mHz biasing frequencies. A large change in τ is indicative of a physicochemical transition induced by increasing charge density to the point where intermolecular interactions at the lipid-water interface are changed significantly. It has been suggested that stress, which can be induced electrostatically through surface charge storage, is a driver for ion channel induction.[34-37] The fact that τ increases with increases in bias voltage suggests that additional energy must be expended to initiate surface charging, implying that interfacial ions respond in a kinetically slow fashion to strong interfacial forces. Indeed, ion-pairing and related interfacial interactions are essential to the assembly of soft-matter systems.[38-40] For example, vibrational sum frequency spectroscopy measurements have shown that hydrogen bonding[38] and ion pairing/electrostatics[39, 40] drive the structure of self-assembled oligomers at oil/aqueous interfaces. However, given the complexity of the system, we cannot specify how lipid structure (*e.g.*, packing, density, etc.) is changing, nor what changes are taking place within the double-layer structure (*e.g.*, ion adsorption, hydrogen bonding network).

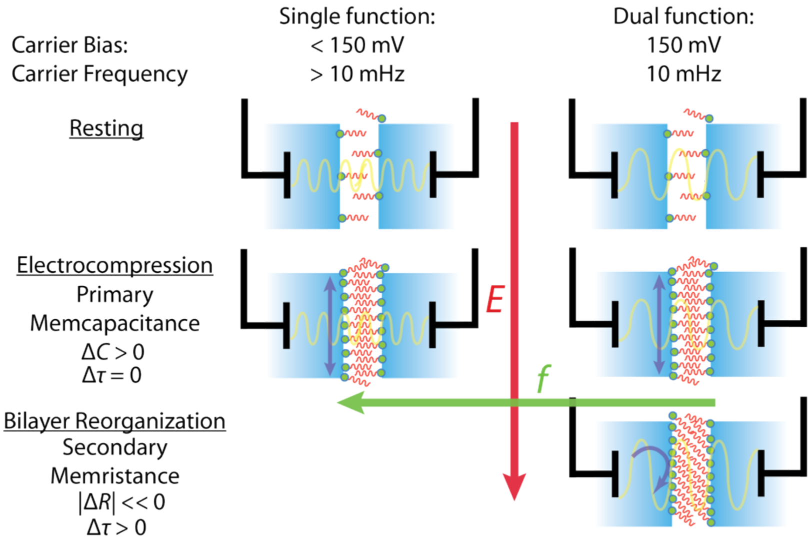

Figure 7. Illustration of the structural evolution of the DPhPC DIB system and resultant electrical properties during a biasing signal between two terminals. Standard singular memcapacitive behavior is observed at small amplitudes and "high" frequencies, whose behavior changes to a dual function at large amplitudes and "low" frequencies.

Figure 7 schematically summarizes how a two-terminal DIB device can be expanded from a single to a multiple memory element device. We note that lipid bilayers are intrinsically asymmetric under an electric field bias. That is, one side will have a more positive charge, while the other will be more negative charged under bias. Given that anions and cations have different solvation structures and transport properties, nonlinear memristance can be tuned and accessed electrically in addition to chemical design. When biasing the DIB using high frequencies (1 Hz > f > 10 mHz) and small amplitudes (< 150 mV), it displays memcapacitive behavior due to electrocompression, whereby the oil is forced out from the fatty lipid layer, reducing membrane thickness.[10] However, by increasing the bias amplitude and decreasing frequency, a secondary effect (dual function) is triggered, driving increased memristance via decoupling of the two memelements. Thus, a two-terminal DIB device has the capability of storing two types of information, high-low capacitance and high-low time-constant values, where the read-write cycles are defined by voltage cycling (memcapacitance) and amplitude/frequency modulation (memristance/time constant). Successful implementation of multiple memelement functionalities into a single two-terminal device will most likely require disentanglement of memcapacitance and memristance signals. The implementation of dEIS into the DIB platform will enable this capability.

Conclusion:

Lipid bilayers are being developed as neuromorphic platforms with tunable plasticity and diverse functionality. The DIB platform has been used to study memristance and memcapacitance, which are most likely the result of a lipid bilayer acyl chain reorganization and/or headgroup reorganization, which affect its dielectric properties, such as capacitance and dielectric loss (an effective resistance). Here, we show that dEIS not only provides insights into the phenomenological origins of these memory effects, but also enables the deconvolution of these processes. This is an important new finding, since a commonly held assumption has been that memcapacitance and memristance are independent of one another. As we have shown, this assumption is not only incorrect, but it also limits the potential functionality of real devices that could utilize the coupling between memristance and memcapacitance in a two-terminal device.

Time-constant analysis shows that memory processes caused by lipid bilayer thickening or thinning do not affect the observed electrical charge/discharge time constant. However, nonlinear effects brought about by membrane reorganization (head group reorientation and acyl chain restructuring) at large biasing potentials dominate the memristance behavior, resulting in an electrical time constant change. In short, dEIS coupled with circuit analysis provides a means for simultaneously extracting multiple memory elements from a single two-terminal device, thereby multiplexing the circuit's function and its potential computational throughput. Biomimetic systems can be tuned for independent control and detection of these or other chemical/physical changes to impart new memory behaviors and result in a greater understanding of the underlying principles for generating intelligent behavior in both living organisms and synthetic systems.

Supporting Information

Supporting Information is available from the Wiley Online Library or from the author.

Acknowledgements

Dynamic electrochemical impedance (dEIS) measurements on droplet interface bilayers were performed at the Center for Nanophase Materials Sciences, which is a U.S. DOE Office of Science User Facility. Data collection, analysis and manuscript preparation were supported by the U.S. DOE, Office of Science, Basic Energy Sciences, Chemical Sciences, Geosciences, and Biosciences Division, and Materials Sciences and Engineering Division. A portion of this research used resources at the Spallation Neutron Source, a U.S. DOE Office of Science User Facility operated by the Oak Ridge National Laboratory. J. Katsaras would like to thank Fyl Pincus (Department of Physics, University of California, Santa Barbara) and Ralph Lydic (Department of Psychology, University of Tennessee) for many fruitful discussions.

Author Contributions

The manuscript was written through the contributions of all authors. All authors have approved the final version of the manuscript. R.L.S., C.P.C., and J.K. conceived the experiments. R.L.S., H.L.S., Z.L., D.B., and C.P.C. carried out the measurements. B.D. participated in the discussion of the results and chemical interpretation.

Received:
Revised:
Published online:

References

1 A. Tardieu, V. Luzzati and F. C. Reman, *J. Mol. Biol.* 1973, **75**, 711–733.

2 J. D. Nickels, S. Chatterjee, C. B. Stanley, S. Qian, X. Cheng, D. A. A. Myles, R. F. Standaert, J. G. Elkins, and J. Katsaras, *PLOS Biology*, 2017, **15**, e2002214.

3 M. L. Kraft, *Mol. Biol. Cell.*, 2013, **24**, 2765–2768.

4 J. S. O'Brien, and E. L. Sampson, *J. Lipid Res.*, 1965, **6**, 537–544.

5 D. Puchkov and V. Haucke, *Trends Cell. Biol.*, 2013, **23**, 493–503.

6 M. Mayford, S. A. Siegelbaum, and E. R. Kandel, *Cold Spring Harb. Perspect Biol.*, 2012, **4**, a005751.

7 M. P. van den Heuvel, C. J. Stam, R. S. Kahn, and H. E. Hulshoff Pol, *J. Neurosci.*, 2009, **29**, 7619–7624.

8 M. A. Holden, D. Needham, and H. Bayley, *J. Am. Chem. Soc.*, 2007, **129**, 8650–8655.

9 J. S. Najem, G. J. Taylor, R. J. Weiss, M. S. Hasan, G. Rose, C. D. Schuman, A. Belianinov, C. P. Collier, and S. A. Sarles, *ACS Nano*, 2018, **12**, 4702–4711.

10 J. S. Najem, M. S. Hasan, R. S. Williams, R. J. Weiss, G. S. Rose, G. J. Taylor, S. A. Sarles and C. P. Collier, *Nature Commun.*, 2019, **10**, 3239.

11 A. Sebastian, M. Le Gallo, R. Khaddam-Aljameh and E. Eleftheriou, *Nature*, 2020, **15**, 529–544.

12 Y. Watanabe, S. Kobayashi, I. Sugiyama, K. Nishio, W. Liu, S. Watanabe, R. Shimizu, and T. Hitosugi, *ACS Appl. Mater. Interfaces*, 2019, **11**, 45150–45154.

13 S.T. Keene, A. Melianas, E.J. Fuller, Y. van de Burgt, A.A. Talin, A. Salleo, *J. Phys. D: Appl. Phys.* 2018, **51**, 224002.

14 A. Lasia, *Electrochemical Impedance Spectroscopy and Its Applications*, Springer, New York, NY, 2014.

15 A. A. Moya, *J. Phys. Chem. C*, 2016, **120**, 6543–6552.

16 M. Legin, G. Laputková, J. Sabo and L. Vojcíková, *Physiol. Res.*, 2007, **56 Suppl 1**, S85–S91.

17 R. L. Sacci and D. A. Harrington, *ECS Transactions*, 2009, **19**, 31–42.

18 R. L. Sacci, F. Seland, and D. A. Harrington, *Electrochim. Acta*, 2014, **131**, 13–19.

19 M. Di Ventra, Y. V. Pershin, and L. O. Chua, *Proc. IEEE*, 2009, **97**, 1717–1724.

20 L. Chua, *Semicond. Sci. Technol.*, 2014, **29**, 104001.

21 J. El-Beyrouthy and E. Freeman, *Membranes (Basel)*, 2021, **11**, 319.

22 G. S. Popkirov, *Electrochim. Acta*, 1996, **41**, 1023–1027.

23 G. S. Popkirov, *J. Electroanal. Chem.*, 1993, **359**, 97–103.

24 J. E. Garland, C. M. Pettit, and D. Roy, *Electrochim. Acta*, 2004, **49**, 2623–2635.

25 D. D. Macdonald, E. Sikora and G. Engelhardt, *Electrochim. Acta.*, 1998, **43**, 87–107.

26 D. D. Macdonald, *Electrochim. Acta*, 2006, **51**, 1376–1388.

27 G. Ragoisha and A. Bondarenko, *Electrochim. Acta*, 2005, **50**, 1553–1563.

28 G. S. Popkirov and R. N. Schindler, *Review of Scientific Instruments*, 1992, **63**, 5366–5372.

29 W. L. Underkofler and I. Shain, *Anal. Chem*, 1965, **37**, 218–222.

30 M. Urquidi-Macdonald, S. Real and D. D. Macdonald, *Electrochim. Acta*, 1990, **35**, 1559–1566.

31 B. A. Boukamp, *J. Electrochem. Soc.*, 1995, **142**, 1885.

32 B. Hirschorn, M. E. Orazem, B. Tribollet, V. Vivier, I. Frateur and M. Musiani, *Electrochim. Acta*, 2010, **55**, 6218–6227.

33 B. Hirschorn, M. E. Orazem, B. Tribollet, V. Vivier, I. Frateur and M. Musiani, *J. Electrochem. Soc.*, 2010, **157**, C452–6.

34 R. Friedman, S. Khalid, C. Aponte-Santamaría, E. Arutyunova, M. Becker, K. J. Boyd, M. Christensen, J. T. S. Coimbra, S. Concilio, C. Daday, F. J. van Eerden, P. A. Fernandes, F. Gräter, D. Hakobyan, A. Heuer, K. Karathanou, F. Keller, M. J. Lemieux, S. J. Marrink, E. R. May, A. Mazumdar, R. Naftalin, M. Pickholz, S. Piotto, P. Pohl, P. Quinn, M. J. Ramos, B. Schiøtt, D. Sengupta, L. Sessa, S. Vanni, T. Zeppelin, V. Zoni, A.-N. Bondar and C. Domene, *J. Membr. Biol.*, 2018, **251**, 609–631.

35 V. E. Zakhvataev, *J. Chem. Phys.*, 2019, **151**, 234902.

36 C. Aponte-Santamaría, J. Brunken and F. Gräter, *J. Am. Chem. Soc*, 2017, **139**, 13588–13591.

37 D. Bolmatov, D. Soloviov, M. Zhernenkov, D. Zav'yalov, E. Mamontov, A. Suvorov, Y. Q. Cai, and J. Katsaras, *Langmuir*, 2020, **36**, 4887–4896.

38 E. J. Robertson, A. P. Carpenter, C. M. Olson, R. K. Ciszewski and G. L. Richmond, *Anal. Chem.*, 2014, **118**, 15260–15273.

39 E. J. Robertson and G. L. Richmond, *Anal. Chem.*, 2014, **118**, 28331–28343.

40 A. U. Chowdhury, L. Lin and B. Doughty, *ACS Appl. Mater. Interfaces*, 2020, **12**, 32119–32130.